



CHORUS

This is the accepted manuscript made available via CHORUS. The article has been published as:

Enhanced valley polarization of graphene on h -BN under circularly polarized light irradiation

Keisuke Nakagahara and Katsunori Wakabayashi

Phys. Rev. B **106**, 075403 — Published 3 August 2022

DOI: [10.1103/PhysRevB.106.075403](https://doi.org/10.1103/PhysRevB.106.075403)

Enhanced valley polarization of graphene on hBN under circularly polarized light irradiation

Keisuke Nakagahara¹ and Katsunori Wakabayashi^{1,2,3}

¹*Department of Nanotechnology for Sustainable Energy, School of Science and Technology, Kwansei Gakuin University, Gakuen-Uegahara 1, Sanda 669-1330, Japan*

²*National Institute for Materials Science (NIMS), Namiki 1-1, Tsukuba 305-0044, Japan and*

³*Center for Spintronics Research Network (CSRN), Osaka University, Toyonaka 560-8531, Japan*

Graphene on hBN (G/hBN) has a long period moiré superstructure owing to the lattice mismatch between two materials. Long periodic potential caused by the moiré superstructure induces modulation of electronic properties of the system. In this paper, we numerically calculate optical conductivity of G/hBN under circularly polarized light irradiation. The lack of spatial inversion symmetry in G/hBN induces the valley polarization. In further, the valley polarization becomes most pronounced in the infrared and terahertz regions if the twist angle between two materials is close to zero for non-doping case, however, insensitive with twist angle for hole-doped case. These results will serve to design the valleytronics devices using G/hBN.

Two-dimensional (2D) atomically-thin materials are attracting much attention owing to its high flexibility to control the electronic and optical properties to design new functional devices[1–4]. Graphene, one atomic thickness carbon sheet, is one of the fundamental 2D materials[5]. Since graphene has honeycomb lattice structure, and its electronic states near the Fermi energy are well described by massless Dirac equation[6, 7]. When two graphenes are overlaid with slight twisting angle, the moiré superstructure appears and works as the long periodic electronic potential for Dirac electrons of graphene [8–15], i.e., so-called *twisted bilayer graphene* (TBG). The period of the moiré superstructure becomes larger with decreasing the twist angle. TBG provides attractive properties such as vanishing the Fermi velocity[11], flat band at the magic angle[16–18] and superconductivity[19–21]. In addition to TBGs, moiré superstructure also appears when different materials are overlaid. Graphene on hBN (G/hBN), i.e., graphene overlaid on hexagonal boron nitride (hBN), has moiré superstructure owing to the mismatch of lattice constants between two materials[22–24]. Experiments of G/hBN have revealed many intriguing phenomena such as the Hofstadter butterfly[25, 26] and the fractional quantum Hall effect [24, 27, 28].

Meanwhile, 2D materials with honeycomb lattice structure such as graphene and hBN have local minima in the conduction band and local maxima in the valence band in the momentum space, which are referred as *valley*. Recently much efforts are devoted to manipulate the valley degree of freedom to encode and process information, i.e., *valleytronics*, which is valley analogue of spintronics[3, 29–35]. The irradiation of circular polarized light onto 2D materials is one of representative ways to generate the valley polarized states[30, 36–40]. Since the broken spatial inversion symmetry is needed to induce valley polarization, the valley polarized states can not be realized in monolayer graphene which respects the spatial inversion symmetry. However, the moiré superlattice potential of G/hBN owing to the lattice mis-

match has the trigonal symmetry, i.e., no inversion symmetry, resulting in the valley polarization. Several groups have recently investigated the electronic properties of G/hBN[41–43], and optical absorption properties[44–47]. However, the optical properties under circular polarized light in G/hBN have not been investigated yet. In this paper, we numerically calculate optical conductivity under circular polarized light irradiation in G/hBN heterostructure. It is shown that the valley polarization is induced in G/hBN owing to the lack of spatial inversion symmetry. In further, the valley polarization becomes most pronounced when the twist angle between graphene and hBN is close to zero for non-doping case. However, for hole-doped case, the valley polarization is insensitive to the twist angle.

Figure 1(a) shows crystal structure of G/hBN with a twist angle $\theta = 0^\circ$, where moiré superstructure is clearly seen owing to the lattice mismatch. \mathbf{L}_1^M and \mathbf{L}_2^M are moiré primitive vectors and the area surrounded by rhombus indicates moiré unit cell. The lattice constant of graphene is $a = 0.246$ nm. Though hBN has the same honeycomb lattice structure, the lattice constant of hBN is $a_{\text{hBN}} = 0.2504$ nm[42, 48], which is slightly larger than graphene. The ratio of lattice constant between graphene and hBN is $\alpha = a_{\text{hBN}}/a \approx 1.018$. When we define $\mathbf{a}_1 = a(1, 0)$ and $\mathbf{a}_2 = a(1/2, \sqrt{3}/2)$ as the primitive vectors of graphene, the primitive vectors of hBN layer of G/hBN are defined as $\tilde{\mathbf{a}} = \alpha R(\theta)\mathbf{a}_i$ ($i = 1, 2$), where $R(\theta)$ is the rotation matrix by angle θ . We define the reciprocal vectors $\mathbf{G}_i, \tilde{\mathbf{G}}_i$ for graphene and hBN, respectively. These vectors should satisfy the relation $\mathbf{a}_i \cdot \mathbf{G}_j = \tilde{\mathbf{a}}_i \cdot \tilde{\mathbf{G}}_j = 2\pi\delta_{ij}$.

The reciprocal vectors for moiré period of G/hBN can be defined as

$$\mathbf{G}_i^M = (\mathbf{1} - \alpha^{-1}R(\theta))\mathbf{G}_i. \quad (1)$$

Note that the period of the moiré superstructure also depends on twist angle. The corresponding moiré primitive vectors satisfy the relation

$$\mathbf{L}_i^M \cdot \mathbf{G}_j^M = 2\pi\delta_{ij}. \quad (2)$$

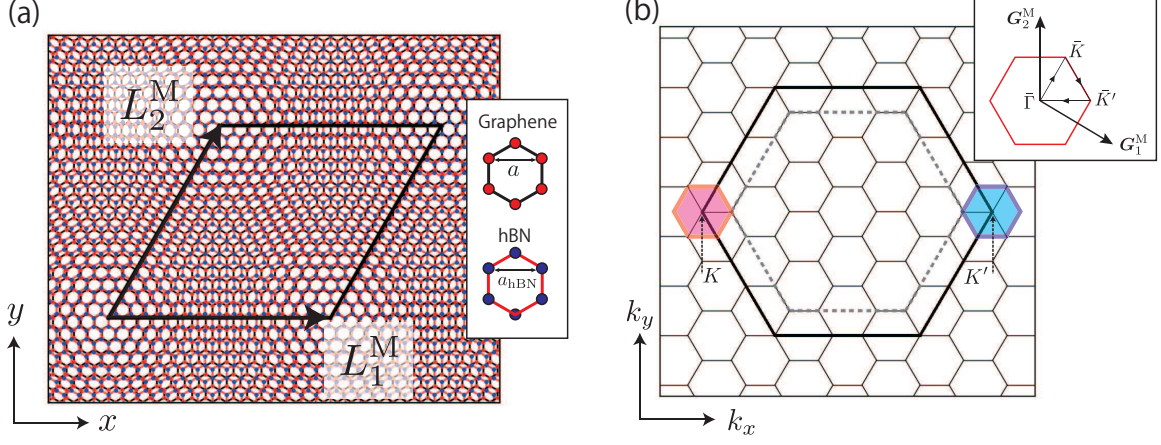


FIG. 1. (a) Crystal structure of G/hBN in real space for twist angle $\theta = 0^\circ$. Here, $a_{\text{hBN}}/a = 16/15$ is used to draw the figure for simplicity. (b) Schematic of reciprocal space. Here, $a_{\text{hBN}}/a = 5/4$ is used to draw the figure for simplicity. Bold black hexagon with a thick line and gray dashed hexagon show the 1st BZ for graphene and hBN, respectively. Small hexagons are moiré BZ. The inset is zoom of moiré BZ.

Long periodic potential appears due to the moiré superstructure and affects on the electronic states of G/hBN. Figure 1(b) shows the schematic of reciprocal space for G/hBN. Bold black hexagon with a thick line and gray dashed hexagon show the 1st BZ for graphene and hBN, respectively. The small hexagons are moiré BZ spanned by \mathbf{G}_1^M and \mathbf{G}_2^M . The inset is the zoom of moiré BZ, where $\bar{\Gamma}$ point means original K (K') point of graphene. In the continuum model, K and K' valleys are treated independently, and the energy bands can be separately plotted in the BZ centered at K (magenta hexagon) and that centered at K' (cyan hexagon).

The electronic states near the Fermi energy of G/hBN are governed by the electronic states of graphene near K and K' points. In this paper, we employ effective continuum model to calculate eigenenergies and eigenfunctions of G/hBN[42]. The K points of graphene are located at $K_\xi = -\xi(2\mathbf{G}_1 + \mathbf{G}_2)/3$, where $\xi = \pm 1$ for K and K' , respectively. The Dirac Hamiltonian of monolayer graphene near K_ξ can be written as

$$H_G = -\hbar v \mathbf{k} \cdot \boldsymbol{\sigma}_\xi, \quad (3)$$

where $\mathbf{k} = (k_x, k_y)$ is the wave number measured from K_ξ point, and $\boldsymbol{\sigma}_\xi = (\xi\sigma_x, \sigma_y)$ with Pauli matrices σ_x and σ_y . H_G is 2×2 matrix for the basis $\{A_\xi, B_\xi\}$, i.e., sublattice degree of freedom of graphene. The parameter v is group velocity of the Dirac cone, which is given as $v = 0.80 \times 10^6$ m/s[42]. By eliminating the basis for hBN using second-order perturbation theory, the effective 2×2 Hamiltonian of G/hBN is written as

$$H_{G/\text{hBN}} = H_G + V_{\text{hBN}}, \quad (4)$$

where V_{hBN} is the long periodic moiré potential including

the effect of hBN. V_{hBN} is given as

$$V_{\text{hBN}} = V_0 \begin{pmatrix} 1 & 0 \\ 0 & 1 \end{pmatrix} + \left\{ V_1 e^{i\xi\psi} \left[\begin{pmatrix} 1 & \omega^{-\xi} \\ 1 & \omega^{-\xi} \end{pmatrix} e^{i\xi\mathbf{G}_1^M \cdot \mathbf{r}} + \begin{pmatrix} 1 & \omega^\xi \\ \omega^\xi & \omega^{-\xi} \end{pmatrix} e^{i\xi\mathbf{G}_2^M \cdot \mathbf{r}} + \begin{pmatrix} 1 & 1 \\ \omega^{-\xi} & \omega^{-\xi} \end{pmatrix} e^{i\xi\mathbf{G}_3^M \cdot \mathbf{r}} \right] + \text{H.c.} \right\},$$

where $\mathbf{G}_3^M = -(\mathbf{G}_1^M + \mathbf{G}_2^M)$, $v = 0.80 \times 10^6$ m/s, $V_0 = 0.0289$ eV, $V_1 = 0.0210$ eV, and $\psi = -0.29$ (rad)[42]. Owing to V_{hBN} , a state at \mathbf{k} is related to the other states at $\mathbf{k} + n_1\mathbf{G}_1^M$, $\mathbf{k} + n_2\mathbf{G}_2^M$, and $\mathbf{k} + n_3\mathbf{G}_3^M$, where n_1, n_2, n_3 are integers. In numerical calculation for optical conductivity, we have taken up to 2th nearest reciprocal lattices, i.e. 19 independent reciprocal lattice vectors, which are the enough number to discuss the low-energy properties of G/hBN system. Thus, the matrix size for numerical calculations is 38×38 .

Figure 2 shows the energy band structure of G/hBN obtained by using continuum model. When the twist angle gets smaller, the electronic states of G/hBN are modulated by long periodic moiré potential. At Brillouin zone boundary, energy band gaps appear in valence bands caused by Bragg scattering where Bloch waves are mixed by moiré periodic potential. Owing to the moiré periodic potential, energy band gap opens about 20 meV at hole band side. The position of the energy band gap goes down with increasing the twist angle. Also, it is noted that a tiny energy band gap with 2 meV is also opened at $E = 0$.

We use Kubo formula to calculate optical conductivity

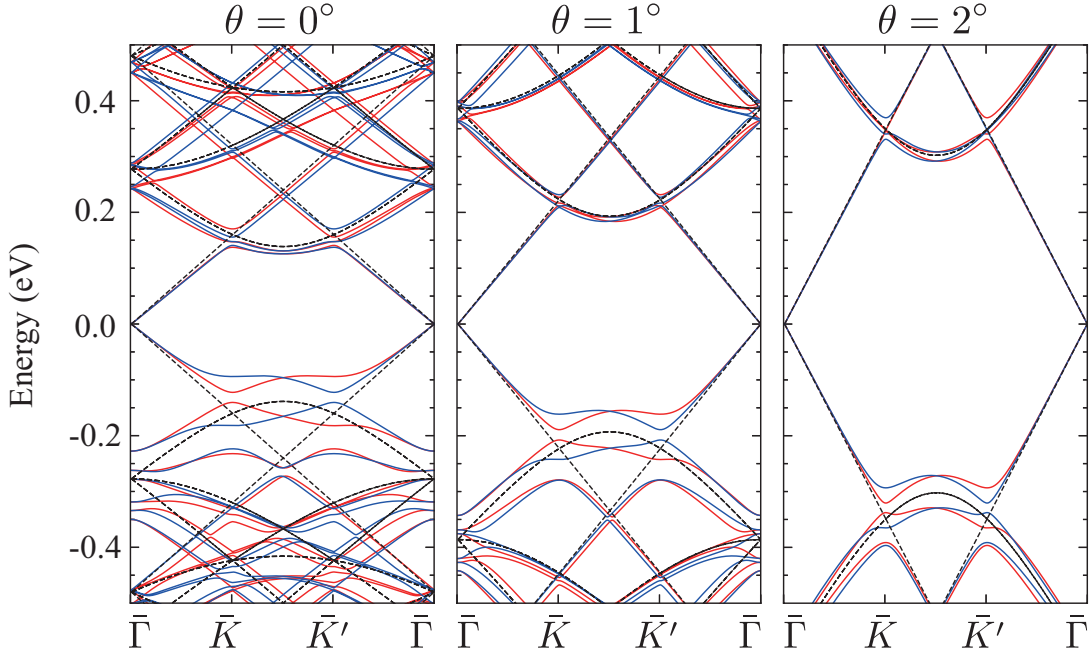


FIG. 2. Energy band structure of G/hBN. Magenta (cyan) bands show the energy bands for K (K') valley and black dashed lines are energy bands of monolayer graphene.

of G/hBN. According to the linear response theory[49], the optical conductivity under the light irradiation which has the frequency ω is given by

$$\sigma(\omega) = \frac{g_s g_v e^2}{i\hbar S} \sum_{i,j} \sum_{\mathbf{k}} \frac{f(E_{\mathbf{k}i}) - f(E_{\mathbf{k}j})}{E_{\mathbf{k}j} - E_{\mathbf{k}i}} \times \frac{|\mathbf{e} \cdot \langle \psi_{\mathbf{k}j} | \nabla_{\mathbf{k}} H | \psi_{\mathbf{k}i} \rangle|^2}{E_{\mathbf{k}j} - E_{\mathbf{k}i} - \hbar\omega - i\eta}, \quad (5)$$

where g_s (g_v) is spin (valley) degree of freedom, i, j are band indices, \mathbf{k} is the wavenumber, $E_{\mathbf{k}i}$ is the eigenenergy for band index i , $\psi_{\mathbf{k}i}$ is the eigenfunction for band index i , S is the area of the system, and $f(E)$ is Fermi-Dirac distribution function. η is an infinitesimally small real number. The vector \mathbf{e} is the polarization vector of incident light. Under left-handed circular polarized light (LCP) irradiation, we use

$$\mathbf{e}_{\text{LCP}} = \frac{1}{\sqrt{2}}(1, i), \quad (6)$$

and under right-handed circular polarized light (RCP) irradiation, we use

$$\mathbf{e}_{\text{RCP}} = \frac{1}{\sqrt{2}}(1, -i). \quad (7)$$

The matrix element of interband transition

$\langle \psi_{\mathbf{k}j} | \nabla_{\mathbf{k}} H | \psi_{\mathbf{k}i} \rangle$ is related to dipole vector $\mathbf{D}(\mathbf{k})$

$$\mathbf{D}(\mathbf{k}) := \langle \psi_{\mathbf{k}j} | \nabla_{\mathbf{r}} | \psi_{\mathbf{k}i} \rangle \quad (8)$$

$$= \frac{i}{\hbar} \langle \psi_{\mathbf{k}j} | \mathbf{p} | \psi_{\mathbf{k}i} \rangle \quad (9)$$

$$= i \frac{m}{\hbar^2} \langle \psi_{\mathbf{k}j} | \nabla_{\mathbf{k}} H | \psi_{\mathbf{k}i} \rangle, \quad (10)$$

where $\psi_{\mathbf{k}i}$ is a state of the valence band and $\psi_{\mathbf{k}j}$ is a state of the conduction band, respectively. $\mathbf{p} = -i\hbar\nabla_{\mathbf{r}}$ is the momentum operator and m is the effective mass of electron. Dipole vector $\mathbf{D}(\mathbf{k})$ is a vector quantity which is composed of complex value. When the real and imaginary parts of dipole vector are mutually orthogonal, the circular dichroism under circular polarized light irradiation occurs[50–52]. For monolayer graphene, the behavior of the dynamical conductivity for massless Dirac electron becomes constant value at the universal conductivity[53, 54],

$$\sigma_{\text{mono}} = \frac{g_s g_v e^2}{16 \hbar}. \quad (11)$$

In followings, we scale the optical conductivity of G/hBN by using σ_{mono} as

$$\frac{\sigma(\omega)}{\sigma_{\text{mono}}} = \frac{16}{iS^{\text{M}}} \sum_{i,j} \sum_{\mathbf{k}} \frac{f(E_{\mathbf{k}i}) - f(E_{\mathbf{k}j})}{E_{\mathbf{k}j} - E_{\mathbf{k}i}} \times \frac{|\mathbf{e} \cdot \langle \psi_{\mathbf{k}j} | \nabla_{\mathbf{k}} H | \psi_{\mathbf{k}i} \rangle|^2}{E_{\mathbf{k}j} - E_{\mathbf{k}i} - \hbar\omega - i\eta}, \quad (12)$$

where S^{M} is the area of the moiré periodic unit cell of G/hBN.

Let us consider the optical conductivity of non-doped G/hBN under circular polarized light irradiation for twist angle $\theta = 0^\circ$, where the Fermi energy E_F is 0 eV. Figure 3 (a) shows the optical conductivity of non-doped G/hBN for Hamiltonian with $\xi = +1$. The conductivity depends on the direction of rotation of circular polarized light especially in infrared and terahertz regions. In particular, for photon energy less than 0.1 eV, the difference between LCP and RCP becomes larger. In this energy region, the interband transition from valence to conduction bands is dominant. Figure 3(b) shows the distribution of dipole vectors for non-doped case, i.e., $E_F = 0.0$ eV. It is clearly seen that the real and imaginary parts of dipole vectors are orthogonal at $\bar{\Gamma}$ point. Thus, the circular dichroism is induced by the irradiation of circular polarized light, and responsible for the electron near $\bar{\Gamma}$ point. For the plot of dipole dipole vectors of Eq.(10), we have used the states of highest valence subband as ψ_{ki} below $E_F = 0.0$ eV, and the states of lowest conduction subband as ψ_{kj} above $E_F = 0.0$.

Next we shall consider the optical conductivity of hole-doped G/hBN. Figure 3 (c) shows the optical conductivity with the Fermi energy $E_F = -0.13$ eV, i.e., hole-doping. In the region of $\omega < 0.1$ eV, the difference of optical conductivities between LCP and RCP becomes much larger than the non-doping case. As shown in Fig. 3 (d), the real and imaginary parts of dipole vectors are mutually orthogonal at \bar{K} and \bar{K}' points, which are responsible for the circular dichroism. The results for Hamiltonian with $\xi = -1$ is obtained by converting LCP (RCP) to RCP (LCP), because K' states of graphene have opposite chirality to K states. Here, for the plot of dipole dipole vectors of Eq.(10), we have used the states of highest occupied subband as ψ_{ki} below $E_F = -0.13$ eV, and the states of lowest unoccupied subband as ψ_{kj} above $E_F = -0.13$ eV.

Since the optical conductivity depends on the direction of rotation of circular polarized light, the valley-selective electron excitation is possible in G/hBN. Here, we define valley polarization for each valley as the difference of the

conductivity between LCP and RCP,

$$P(\omega) = \frac{\sigma_L - \sigma_R}{\sigma_L + \sigma_R}, \quad -1 \leq P(\omega) \leq 1, \quad (13)$$

where σ_L and σ_R are the optical conductivity under LCP and RCP, respectively. The positive (negative) value of $P(\omega)$ means that the electron at the valley is easy to excite by LCP (RCP). Figures 4 (a) and (b) show the photon energy dependence of valley polarization for (a) non-doping case and (b) hole-doped case, respectively. In these Figures, the value of $P(\omega)$ is shifted by $+1$ per 1° of twist angle. The black, magenta and cyan curves indicate the case of twist angle $\theta = 0, 1, 2^\circ$. For non-doping case, the value of valley polarization less than 0.1 eV has maximum value for $\theta = 0^\circ$ and it is decreasing with increase of the twist angle. These results indicate that the electronic properties of G/hBN approaches to the electronic states of monolayer graphene with increase of the twist angle. On the other hand, the peak of valley polarization less than 0.1 eV for hole-doped case remains even though the twist angle becomes larger. The common peak of valley polarization comes from interband transition across the Fermi energy E_F at \bar{K} point.

In this paper, we have numerically calculated the optical conductivity of G/hBN under circular polarized light irradiation. The optical conductivity of G/hBN changes their behavior depending on the direction of rotation of circular polarized light due to broken spatial inversion symmetry of the system. By analyzing the dipole vectors, we have confirmed that the real and imaginary parts of dipole vectors are mutually orthogonal. Thus, we can explain that the electron for each valley can be selectively excited by using a certain direction of circular polarized light irradiation. These results indicate that G/hBN can cause valley polarization by circular polarized light irradiation. Also, we confirmed that the value of valley polarization of G/hBN depends on not only twist angle but also Fermi energy. For nondoping case, the peak of valley polarization for photon energy less than 0.1 eV is vanished as larger twist angle. On the other hand, for hole-doped case, it remains even though twist angle becomes larger. These results will serve to design the valleytronics devices using G/hBN.

This work was supported by JSPS KAKENHI (No. JP21H01019, No. 22H05473 and No. JP18H01154) and JST CREST (No. JPMJCR19T1).

-
- [1] K. S. Novoselov, A. Mishchenko, A. Carvalho, and A. H. C. Neto, 2D materials and van der Waals heterostructures, *Science* **353**, 6298 (2016).
 [2] S. Das, J. A. Robinson, M. Dubey, H. Terrones, and M. Terrones, Beyond Graphene: Progress in Novel Two-Dimensional Materials and van der Waals Solids, *Ann. Rev. Mater. Res.* **45**, 1 (2015).
 [3] J. R. Schaibley, H. Yu, G. Clark, P. Rivera, J. S. Ross, K. L. Seyler, W. Yao, and X. Xu, Valleytronics in 2D

- materials, *Nature Rev. Mater.* **1**, 16055 (2016).
 [4] M. Zeng, Y. Xiao, J. Liu, K. Yang, and L. Fu, Exploring Two-Dimensional Materials toward the Next-Generation Circuits: From Monomer Design to Assembly Control, *Chem. Rev.* **118**, 6236 (2018).
 [5] A. H. Castro Neto, F. Guinea, N. M. R. Peres, K. S. Novoselov, and A. K. Geim, The electronic properties of graphene, *Rev. Mod. Phys.* **81**, 109 (2009).
 [6] H. Ajiki and T. Ando, Electronic states of carbon nan-

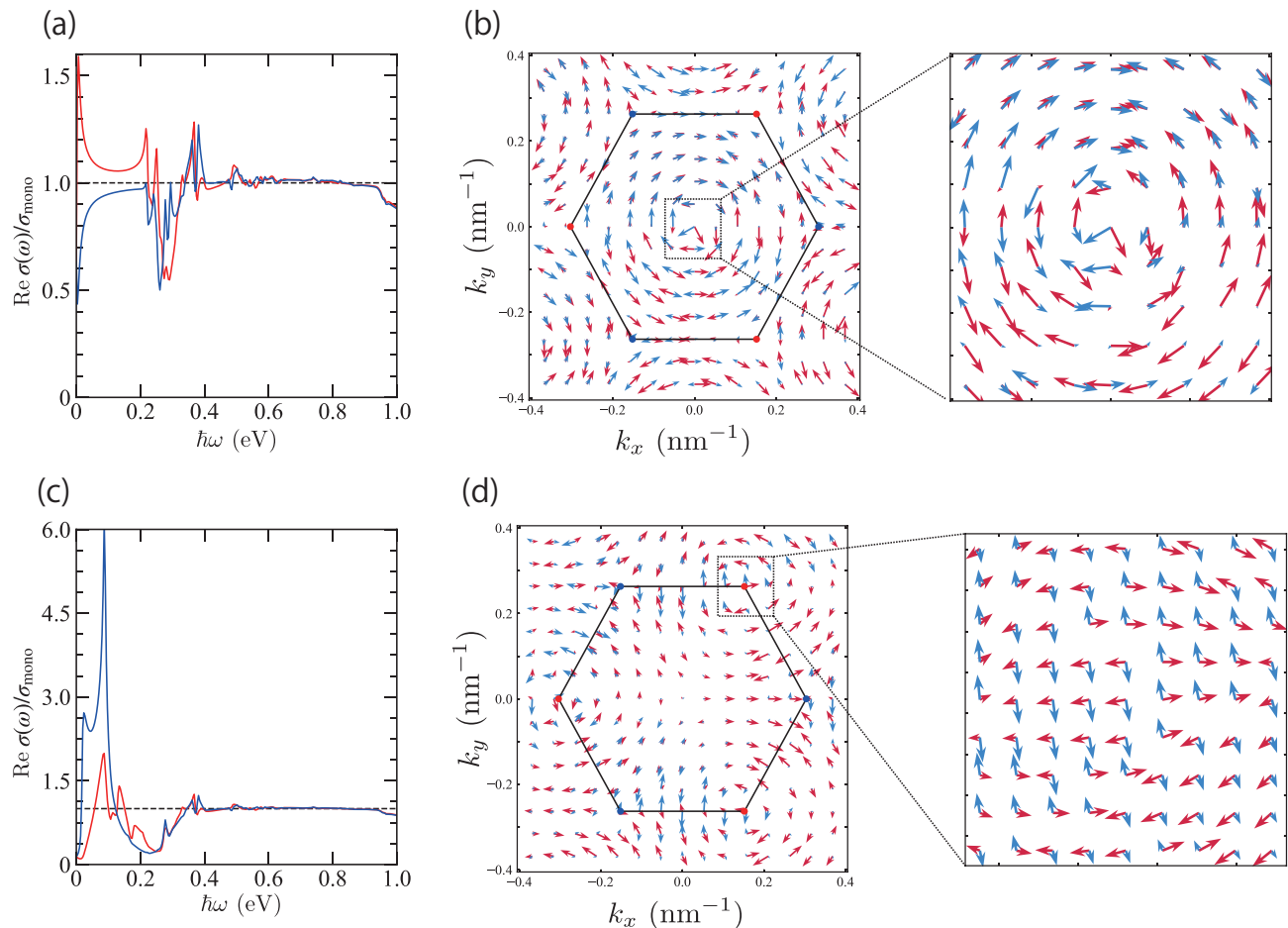


FIG. 3. (a) Optical conductivity of G/hBN for $\xi = 1$ and $E_F = 0.0$ eV under circular polarized light, where the twist angle θ is 0° . Magenta (cyan) curve is the conductivity for LCP (RCP). (b) Distribution of dipole vectors for interband transition near Fermi energy $E_F = 0.0$ eV in momentum space. The magenta (cyan) arrows are the real (imaginary) part of the dipole vectors. Black hexagon is moiré BZ and magenta (cyan) dots at the hexagon corners are \bar{K} (\bar{K}') point. (c) Optical conductivity of G/hBN for $E_F = -0.13$ eV, where the twist angle θ is 0° . (d) Distribution of dipole vectors for interband transition near Fermi energy $E_F = -0.13$ eV in momentum space.

- otubes, *J. Phys. Soc. Jpn.* **62**, 1255 (1993).
- [7] T. Ando, T. Nakanishi, and R. Saito, Berry's phase and absence of back scattering in carbon nanotubes, *J. Phys. Soc. Jpn.* **67**, 2857 (1998).
- [8] J. M. B. Lopes dos Santos, N. M. R. Peres, and A. H. Castro Neto, Graphene bilayer with a twist: Electronic structure, *Phys. Rev. Lett.* **99**, 256802 (2007).
- [9] G. Trambly de Laissardière, D. Mayou, and L. Magaud, Localization of dirac electrons in rotated graphene bilayers, *Nano Lett.* **10**, 804 (2010).
- [10] E. J. Mele, Commensuration and interlayer coherence in twisted bilayer graphene, *Phys. Rev. B* **81**, 161405(R) (2010).
- [11] R. Bistritzer and A. H. MacDonald, Moiré bands in twisted double-layer graphene, *Proc. Natl. Acad. Sci.* **108**, 12233 (2011).
- [12] E. Suárez Morell, J. D. Correa, P. Vargas, M. Pacheco, and Z. Barticevic, Flat bands in slightly twisted bilayer graphene: Tight-binding calculations, *Phys. Rev. B* **82**, 121407(R) (2010).
- [13] P. Moon and M. Koshino, Energy spectrum and quantum hall effect in twisted bilayer graphene, *Phys. Rev. B* **85**, 195458 (2012).
- [14] J. M. B. Lopes dos Santos, N. M. R. Peres, and A. H. Castro Neto, Continuum model of the twisted graphene bilayer, *Phys. Rev. B* **86**, 155449 (2012).
- [15] P. Moon and M. Koshino, Optical absorption in twisted bilayer graphene, *Phys. Rev. B* **87**, 205404 (2013).
- [16] M. I. B. Utama, R. J. Koch, K. Lee, N. Leconte, H. Li, S. Zhao, L. Jiang, J. Zhu, K. Watanabe, T. Taniguchi, P. D. Ashby, A. Weber-Bargioni, A. Zettl, C. Jozwiak, J. Jung, E. Rotenberg, A. Bostwick, and F. Wang, Visualization of the flat electronic band in twisted bilayer graphene near the magic angle twist, *Nature Phys.* **17**, 184 (2021).
- [17] S. Lisi, X. Lu, T. Benschop, T. A. d. Jong, P. Stepanov, J. R. Duran, F. Margot, I. Cucchi, E. Cappelli, A. Hunter, A. Tamai, V. Kandyba, A. Giampietri, A. Barinov, J. Jobst, V. Stalman, M. Leeuwenhoek, K. Watanabe, T. Taniguchi, L. Rademaker, S. J. v. d.

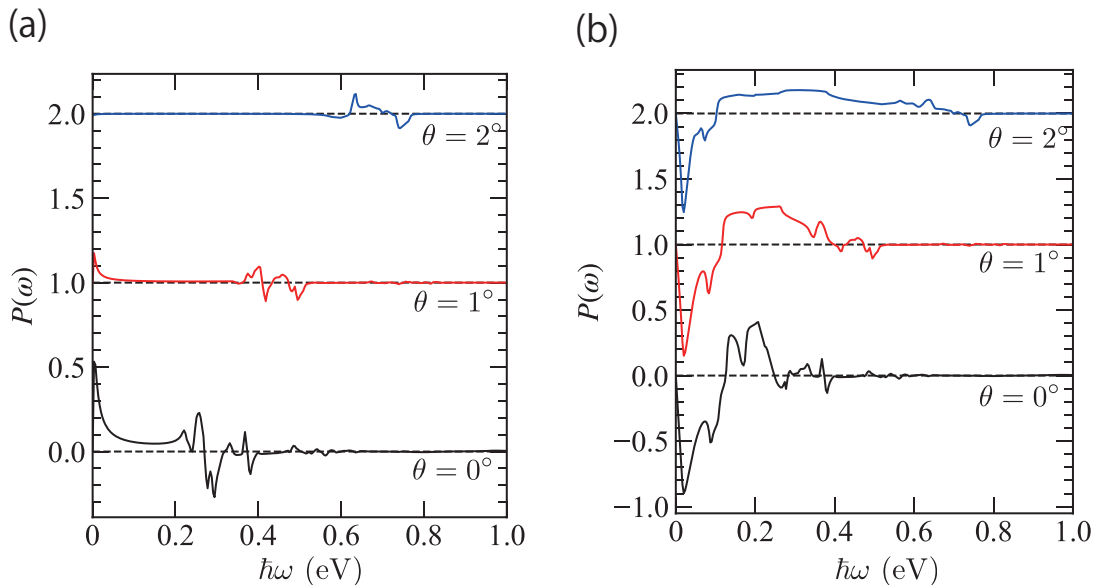


FIG. 4. (a) Photon energy dependence of valley polarization ($E_F = 0$ for several different twist angles. eV). Black dashed lines indicate $P(\omega) = 0$ line. (b) Photon energy dependence of valley polarization for hole-doped case, where the Fermi energy is set in the bandgap of the valence band at K point. Fermi energies are set $E_F = -0.13$ eV for $\theta = 0^\circ$, $E_F = -0.20$ eV for $\theta = 1^\circ$, and $E_F = -0.33$ eV for $\theta = 2^\circ$.

- Molen, M. P. Allan, D. K. Efetov, and F. Baumberger, Observation of flat bands in twisted bilayer graphene, *Nature Phys.* **17**, 189 (2021).
- [18] K. Sato, N. Hayashi, T. Ito, N. Masago, M. Takamura, M. Morimoto, T. Maekawa, D. Lee, K. Qiao, J. Kim, K. Nakagahara, K. Wakabayashi, H. Hibino, and W. Norimatsu, Observation of a flat band and bandgap in millimeter-scale twisted bilayer graphene, *Communications Materials* **2**, 117 (2021).
- [19] Y. Cao, V. Fatemi, A. Demir, S. Fang, S. L. Tomarken, J. Y. Luo, J. D. Sanchez-Yamagishi, K. Watanabe, T. Taniguchi, E. Kaxiras, R. C. Ashoori, and P. Jarillo-Herrero, Correlated insulator behaviour at half-filling in magic-angle graphene superlattices, *Nature* **556**, 80 (2018).
- [20] Y. Cao, V. Fatemi, S. Fang, K. Watanabe, T. Taniguchi, E. Kaxiras, and P. Jarillo-Herrero, Unconventional superconductivity in magic-angle graphene superlattices, *Nature* **556**, 43 (2018).
- [21] M. Yankowitz, S. Chen, H. Polshyn, Y. Zhang, K. Watanabe, T. Taniguchi, D. Graf, A. F. Young, and C. R. Dean, Tuning superconductivity in twisted bilayer graphene, *Science* **363**, 1059 (2019).
- [22] G. J. Slotman, M. M. van Wijk, P.-L. Zhao, A. Fasolino, M. I. Katsnelson, and S. Yuan, Effect of structural relaxation on the electronic structure of graphene on hexagonal boron nitride, *Phys. Rev. Lett.* **115**, 186801 (2015).
- [23] M. M. van Wijk, A. Schuring, M. I. Katsnelson, and A. Fasolino, Moiré patterns as a probe of interplanar interactions for graphene on h-bn, *Phys. Rev. Lett.* **113**, 135504 (2014).
- [24] M. Yankowitz, Q. Ma, P. Jarillo-Herrero, and B. J. LeRoy, van der Waals heterostructures combining graphene and hexagonal boron nitride, *Nature Rev. Phys.* **1**, 112 (2019).
- [25] C. R. Dean, L. Wang, P. Maher, C. Forsythe, F. Ghahari, Y. Gao, J. Katoch, M. Ishigami, P. Moon, M. Koshino, T. Taniguchi, K. Watanabe, K. L. Shepard, J. Hone, and P. Kim, Hofstadter's butterfly and the fractal quantum Hall effect in moiré superlattices, *Nature* **497**, 598 (2013).
- [26] B. Hunt, J. D. Sanchez-Yamagishi, A. F. Young, M. Yankowitz, B. J. LeRoy, K. Watanabe, T. Taniguchi, P. Moon, M. Koshino, P. Jarillo-Herrero, and R. C. Ashoori, Massive Dirac Fermions and Hofstadter Butterfly in a van der Waals Heterostructure, *Science* **340**, 1427 (2013).
- [27] L. Wang, Y. Gao, B. Wen, Z. Han, T. Taniguchi, K. Watanabe, M. Koshino, J. Hone, and C. R. Dean, Evidence for a fractional fractal quantum Hall effect in graphene superlattices, *Science* **350**, 1231 (2015).
- [28] L. Balents, C. R. Dean, D. K. Efetov, and A. F. Young, Superconductivity and strong correlations in moiré flat bands, *Nature Physics*, 1 (2020).
- [29] A. Rycerz, J. Tworzydo, and C. W. J. Beenakker, Valley filter and valley valve in graphene, *Nature Phys.* **3**, 172 (2007).
- [30] D. Xiao, G.-B. Liu, W. Feng, X. Xu, and W. Yao, Coupled spin and valley physics in monolayers of MoS_2 and other group-VI dichalcogenides, *Phys. Rev. Lett.* **108**, 196802 (2012).
- [31] X. Xu, W. Yao, D. Xiao, and T. F. Heinz, Spin and pseudospins in layered transition metal dichalcogenides, *Nature Phys.* **10**, 343 (2014).
- [32] Y. P. Shkolnikov, E. P. De Poortere, E. Tutuc, and M. Shayegan, Valley splitting of 2D electrons in a perpendicular magnetic field, *Phys. Rev. Lett.* **89**, 226805 (2002).
- [33] J. Isberg, M. Gabrysch, J. Hammersberg, S. Majidi, K. K. Kovi, and D. J. Twitchen, Generation, transport and detection of valley-polarized electrons in diamond, *Nature*

- Materials **12**, 760 (2013).
- [34] Z. Zhu, A. Collaudin, B. Fauqu, W. Kang, and K. Behnia, Field-induced polarization of Dirac valleys in bismuth, *Nature Physics* **8**, 89 (2012), 1109.2774.
- [35] Y. Shimazaki, M. Yamamoto, I. V. Borzenets, K. Watanabe, T. Taniguchi, and S. Tarucha, Generation and detection of pure valley current by electrically induced Berry curvature in bilayer graphene, *Nature Phys.* **11**, 1032 (2015).
- [36] W. Yao, D. Xiao, and Q. Niu, Valley-dependent optoelectronics from inversion symmetry breaking, *Phys. Rev. B* **77**, 235406 (2008).
- [37] T. Cao, G. Wang, W. Han, H. Ye, C. Zhu, J. Shi, Q. Niu, P. Tan, E. Wang, B. Liu, and J. Feng, Valley-selective circular dichroism of monolayer molybdenum disulphide, *Nature Comm.* **3**, 887 (2012).
- [38] H. Zeng, J. Dai, W. Yao, D. Xiao, and X. Cui, Valley polarization in MoS2 monolayers by optical pumping, *Nature Nanotech.* **7**, 490 (2012).
- [39] K. F. Mak, K. He, J. Shan, and T. F. Heinz, Control of valley polarization in monolayer MoS2 by optical helicity, *Nature Nanotech.* **7**, 494 (2012).
- [40] A. M. Jones, H. Yu, N. J. Ghimire, S. Wu, G. Aivazian, J. S. Ross, B. Zhao, J. Yan, D. G. Mandrus, D. Xiao, W. Yao, and X. Xu, Optical generation of excitonic valley coherence in monolayer WSe2, *Nature Nanotech.* **8**, 634 (2013), 1303.5318.
- [41] J. R. Wallbank, A. A. Patel, M. Mucha-Kruczyński, A. K. Geim, and V. I. Fal'ko, Generic miniband structure of graphene on a hexagonal substrate, *Phys. Rev. B* **87**, 245408 (2013).
- [42] P. Moon and M. Koshino, Electronic properties of graphene/hexagonal-boron-nitride moiré superlattice, *Phys. Rev. B* **90**, 155406 (2014).
- [43] Y. Du, N. Xu, X. Lin, and A.-P. Jauho, Moiré effects in graphene-hbn heterostructures, *Phys. Rev. Research* **2**, 043427 (2020).
- [44] D. S. Abergel, J. Wallbank, X. Chen, M. Mucha-Kruczyński, and V. I. Fal'ko, Infrared absorption by graphene/hbn heterostructures, *New J. Phys.* **15**, 123009 (2013).
- [45] Z. Shi, C. Jin, W. Yang, L. Ju, J. Horng, X. Lu, H. A. Bechtel, M. C. Martin, D. Fu, J. Wu, K. Watanabe, T. Taniguchi, Y. Zhang, X. Bai, E. Wang, G. Zhang, and F. Wang, Gate-dependent pseudospin mixing in graphene/boron nitride moiré superlattices, *Nature Phys.* **10**, 743 (2014).
- [46] D. S. L. Abergel and M. Mucha-Kruczyński, Infrared absorption of closely aligned heterostructures of monolayer and bilayer graphene with hexagonal boron nitride, *Phys. Rev. B* **92**, 115430 (2015).
- [47] A. M. DaSilva, J. Jung, S. Adam, and A. H. MacDonald, Terahertz conductivity of graphene on boron nitride, *Phys. Rev. B* **92**, 155406 (2015).
- [48] L. Liu, Y. P. Feng, and Z. X. Shen, Structural and electronic properties of h-bn, *Phys. Rev. B* **68**, 104102 (2003).
- [49] R. Kubo, Statistical-mechanical theory of irreversible processes. i. general theory and simple applications to magnetic and conduction problems, *J. Phys. Soc. Jpn.* **12**, 570 (1957).
- [50] Y. Tatsumi, K. Ghalamkari, and R. Saito, Laser energy dependence of valley polarization in transition-metal dichalcogenides, *Phys. Rev. B* **94**, 235408 (2016).
- [51] K. Ghalamkari, Y. Tatsumi, and R. Saito, Energy band gap dependence of valley polarization of the hexagonal lattice, *J. Phys. Soc. Jpn.* **87**, 024710 (2018).
- [52] M. Akita, Y. Fujii, M. Maruyama, S. Okada, and K. Wakabayashi, Momentum-selective optical absorption in triptycene molecular membrane, *Phys. Rev. B* **101**, 085418 (2020).
- [53] T. Ando, Y. Zheng, and H. Suzuura, Dynamical conductivity and zero-mode anomaly in honeycomb lattices, *J. Phys. Soc. Jpn.* **71**, 1318 (2002).
- [54] M. Koshino, Stacking-dependent optical absorption in multilayer graphene, *New J. Phys.* **15**, 015010 (2013).